Stem Cell Reports
Article

ISSCR

OPEN ACCESS

PTBP2 attenuation facilitates fibroblast to neuron conversion by promoting alternative splicing of neuronal genes

Binglin Zhu,[1,2,3,4] Emily Fisher,[2,4] Li Li,[2,4] Ping Zhong,[2] Zhen Yan,[1,2] and Jian Feng[1,2,*]
[1]Veterans Affairs Western New York Healthcare System, Buffalo, NY 14215, USA
[2]Department of Physiology and Biophysics, State University of New York at Buffalo, Buffalo, NY 14203, USA
[3]Present address: Jinfeng Laboratory, Chongqing 401329, China
[4]These author contributed equally
*Correspondence: jianfeng@buffalo.edu
https://doi.org/10.1016/j.stemcr.2023.09.012

SUMMARY

The direct conversion of human skin fibroblasts to neurons has a low efficiency and unclear mechanism. Here, we show that the knockdown of *PTBP2* significantly enhanced the transdifferentiation induced by *ASCL1*, MIR9/9*-124, and *p53* shRNA (AMp) to generate mostly GABAergic neurons. Longitudinal RNA sequencing analyses identified the continuous induction of many RNA splicing regulators. Among these, the knockdown of *RBFOX3* (NeuN), significantly abrogated the transdifferentiation. Overexpression of *RBFOX3* significantly enhanced the conversion induced by AMp; the enhancement was occluded by *PTBP2* knockdown. We found that *PTBP2* attenuation significantly favored neuron-specific alternative splicing (AS) of many genes involved in synaptic transmission, signal transduction, and axon formation. *RBFOX3* knockdown significantly reversed the effect, while *RBFOX3* overexpression occluded the enhancement. The study reveals the critical role of neuron-specific AS in the direct conversion of human skin fibroblasts to neurons by showing that *PTBP2* attenuation enhances this mechanism in concert with *RBFOX3*.

INTRODUCTION

Transdifferentiation of readily accessible cells, for example, skin fibroblasts, to inaccessible cells, such as neurons, is an important approach to study human brain disorders (Vierbuchen and Wernig, 2011; Xu et al., 2017). The ability of induced neurons to maintain the epigenetic information imparted by age is a significant advantage over neurons differentiated from induced pluripotent stem cells, particularly in studying neurodegenerative disorders (Mertens et al., 2021). However, the transdifferentiation of human skin fibroblasts to induced neurons has a low efficiency and unclear mechanism (Li et al., 2019). A variety of methods using transgenes, microRNAs, small-molecule compounds, or their combinations have been used for the direct conversion (Xu et al., 2020), for example, ASCL1 (Pang et al., 2011), miR9/9*-124 (Yoo et al., 2011), or short hairpin RNAs (shRNAs) of *PTB* and *nPTB* (Xue et al., 2013, 2016). Our previous studies have shown that the cell cycle and p53 serve as critical barriers (Feng, 2016), as cell-cycle synchronization at the G1/S checkpoint and suppression of p53 markedly improve the transdifferentiation (Jiang et al., 2015). Overexpression of *ASCL1* in mitotic cells, such as skin fibroblasts, induces rapid exit from the cell cycle (Jiang et al., 2015). The neuron-specific *MIR9/9*-124* suppresses Repressor Element-1 Silencing Transcription factor (*REST*), which represses the expression of neuronal genes in non-neuronal cells (Lu and Yoo, 2018), and targets the 3′ UTR of *PTB* and *nPTB* to reduce their expression (Lu et al., 2021). Knockdown of *PTB* converts many types of cells to immature neurons (Xue et al., 2013). The subsequent knockdown of *nPTB* promotes the maturation of these cells and, with the help of *BRN2*, induces the expression of *MAP2* (Xue et al., 2016).

Neurons form complex computational networks by connecting to each other through numerous and specific synapses. A molecular barcoding mechanism must exist to specify the unique identity of a neuron, including various domains of its cell surface, to form precise synaptic connections that number 30,000 per human cortical neuron, for example (DeFelipe et al., 2002). The only biologically plausible mechanism is alternative splicing (AS), which is capable of producing vast combinations of protein variants that interact with their counterparts with almost infinite levels of affinity to establish optimal synaptic connections. AS is particularly active in the brain, producing the most diverse transcripts in all tissues (Mele et al., 2015). Among the 305 RNA splicing regulators (RSRs) that orchestrate AS in humans, only 17 have minimal or no expression in the brain (Fisher and Feng, 2022).

This analysis prompted us to test the idea that the direct conversion of human skin fibroblasts to neurons may require a sequence of events that include cell-cycle exit driven by ASCL1 (Jiang et al., 2015), MIR9/9*-124-mediated suppression of REST (Lu and Yoo, 2018), and the subsequent induction of neuronal genes and neuron-specific AS of these genes for the maturation and stabilization of neuronal fate (Lipscombe and Lopez Soto, 2019). Our results showed that *nPTB* knockdown (n) markedly enhanced the direct conversion of human skin fibroblasts

to neurons by ASCL1, MIR9/9*-124 and p53 shRNA (AMp; capital letters for overexpression and lowercase letters for knockdown). Most of the AMnp-induced neurons were GABAergic. Longitudinal RNA sequencing (RNA-seq) analysis identified the continuous upregulation of many neuronal genes and neuron-specific AS of these genes. Among the continuously up-regulated RSRs, *RBFOX3*, which encodes NeuN (Dredge and Jensen, 2011; Kim et al., 2009), played a critical role in the transdifferentiation. *RBFOX3* knockdown significantly decreased the conversion and neuron-specific AS, while overexpression of *RBFOX3* significantly increased AMp-induced conversion and neuron-specific AS and occluded the enhancing effects of *nPTB* shRNA in AMnp-induced conversion. Our study suggests that the two RSRs, nPTB and RBFOX3, act in a coordinated manner to promote the direct conversion of human skin fibroblasts to neurons by increasing neuron-specific AS of many genes induced in the conversion process, thus driving the maturation of the converted neurons.

RESULTS

PTBP2 knockdown significantly enhances the transdifferentiation of human skin fibroblasts to neurons

Our previous study has shown that cell-cycle arrest at the G1/S checkpoint by serum withdrawal for 24 h, in conjunction with *p53* knockdown, markedly increased the direct conversion of human lung fibroblasts to induced dopaminergic neurons by *ASCL1*, *NURR1*, *LMX1A*, and *MIR124* (Jiang et al., 2015). However, the conversion of human skin fibroblasts to neurons by *ASCL1* and *p53* shRNA is much less efficient (Li et al., 2019). Using the protocol in Figure 1A, we systematically tested the effects of *ASCL1* (A), *MIR9/9*-124* (M) (Victor et al., 2014), *PTBP2* (*nPTB*) shRNA (n) (Xue et al., 2016), or *p53* shRNA (p) either alone or in various combinations (Figures 1B–1Q). The transdifferentiation of AG22056 human skin fibroblasts to neurons required *ASCL1* (Figure 1C); any single factor or their combinations without A failed to generate neurons within 14 days (Figures 1D–1I, and 1M). The addition of M, n, or p significantly enhanced the effect of A to similar degrees (Figure 1C vs. Figure 1J–1L), as quantified by reprogramming yield (Figure 1R) and efficiency (Figure 1S). The combinations of AMn, Amp, and Anp improved reprogramming further (Figures 1N–1P, 1R, and 1S). The most substantial effect was produced by the combination of all four factors (AMnp), with 90.5% ± 5.1% of all cells being TUJ1$^+$ and 52.1% ± 4.0% of all cells being MAP2$^+$ at day 14, without any selection to enrich neurons. The total number of DAPI$^+$ cells was significantly reduced by An, Amn, or Anp in the order of decreasing severity. By itself, n had no significant toxicity; it only became moderately toxic in the presence of A-induced reprogramming. The toxicity was attenuated by M or p and was eliminated by the combination of Mp, as AMnp induced no significant cell loss (Figure 1T). At day 40, AMnp-induced neurons exhibited voltage-gated Na^+ and K^+ currents (Figure 1U) and evoked action potentials (Figure 1V), which confirmed that they were functional neurons.

Rapid pace of AMnp-induced neuronal conversion

At day 3 of reprogramming (Figure 2B), 1.1% ± 0.4% of cells were MAP2$^+$ neurons (Figures 2H and 2N). At day 7, neuronal cells with long processes and multipolar morphology were observed, and the percentage of MAP2$^+$ neurons increased to 15.8% ± 4.2% (Figures 2C, 2I, and 2N). Over time, increasingly more complex morphologies were seen, indicating a process of maturation in AMnp-induced neurons (Figures 2D–2F and 2J–2L). Reprogramming efficiencies in terms of the MAP2$^+$/DAPI$^+$ ratio were similar between day 14 (52.1% ± 4.0%) and day 21 (51.0% ± 7.6%), and increased slightly at day 28 (55.7% ± 5.6%) ($p = 0.3774$) (Figure 2N). From days 14 through 28, the slight decrease in the number of TUJ1$^+$ cells (Figure 2M) paralleled the moderate decrease of DAPI$^+$ cells (Figure 2O), while the number of MAP2$^+$ mature neurons did not change significantly (Figure 2M). It suggests that some of the immature TUJ1$^+$ cells may die with time, while MAP2$^+$ mature neurons persist.

Consistent with our previous finding (Jiang et al., 2015), the expression of lentiviral transgenes *ASCL1*, *MIR124*, and *MIR9*, which are driven by an RNA polymerase II promoter in the FUW vector, was markedly silenced as reprogramming proceeded from day 3 to day 14 (Figure S1A). In contrast, the expression of *PTBP2* shRNA or *p53* shRNA transgene under an RNA polymerase III promoter in the pLKO.1 vector was not significantly affected during reprogramming (Figure S1A). Endogenous *ASCL1*, *MIR124*, and *MIR9* were significantly induced, while endogenous *PTBP2* and *p53* were significantly suppressed during reprogramming (Figure S1B). AMnp was markedly more effective and rapid than the well reported condition of ASCL1, BRN2, MYT1L, and NEUROD1 (Pang et al., 2011) in converting AG22056 human skin fibroblasts to induced neurons (Figures S1C–S1H).

We found that AMnp converted six lines of primary human skin fibroblasts and four lines of primary human lung fibroblasts at varying efficiencies and yields. Three lines of skin fibroblasts, with donor ages including 16 fetal weeks, newborn, and 78 years, showed similarly high conversion yields and efficiencies (Figures S2A–S2C and S2G–S2I). The other three lines of skin fibroblasts, with donor ages including 26 years, 31 years, and 96 years, had much lower conversion yields and efficiencies, which was accompanied

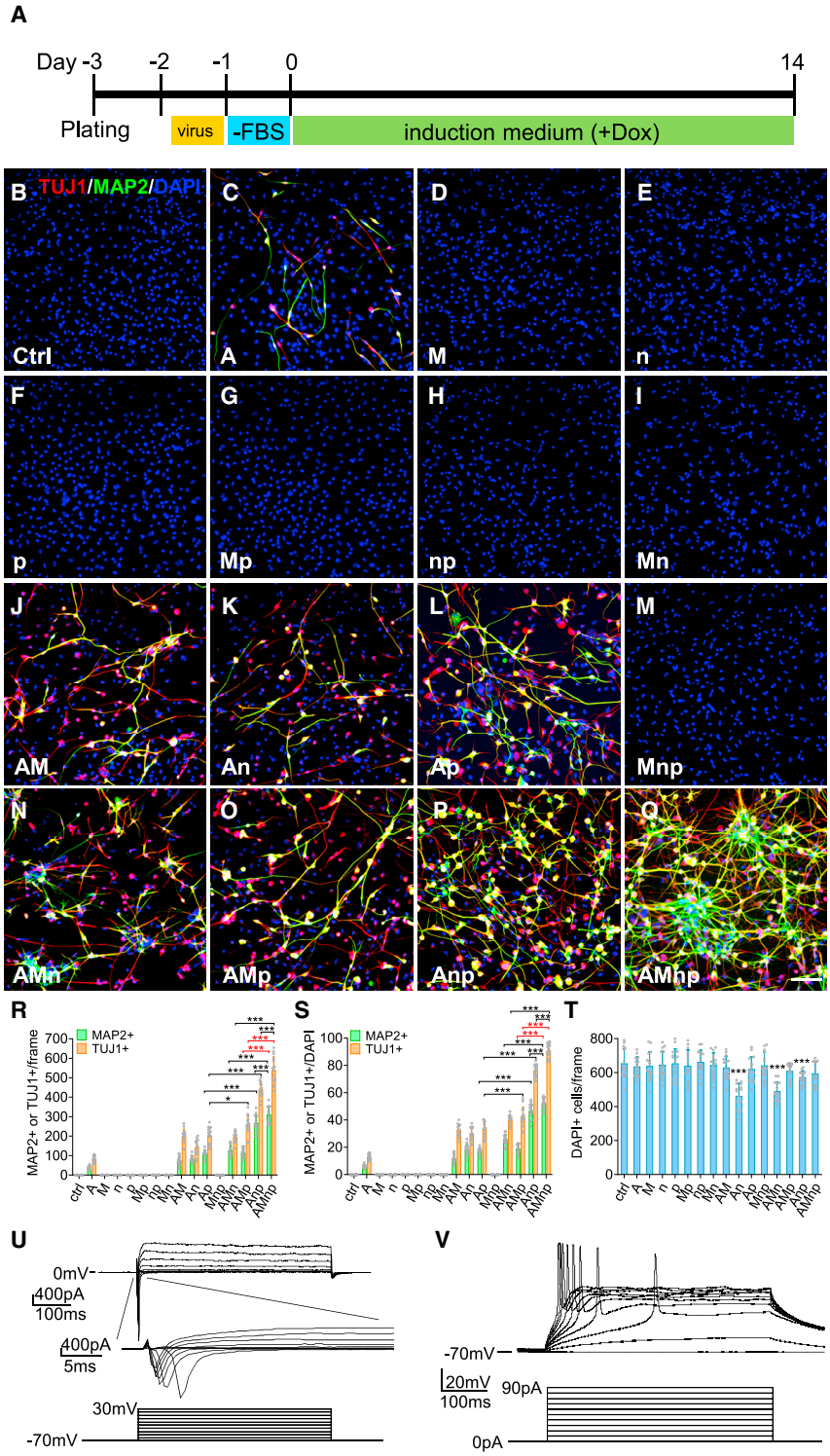

Figure 1. *PTBP2* knockdown enhances the direct conversion of human skin fibroblasts to neurons

(A–Q) Using the reprogramming strategy in (A), AG22056 primary foreskin fibroblasts were reprogrammed to neurons in neural induction medium without (B) or with the indicated combinations of lentiviruses (C–Q) expressing *ASCL1* (A), *MiR9/9*-124* (M), *PTBP2* shRNA (n), and *p53* shRNA (p). Cells at day 14 were stained for MAP2, TUJ1, and DAPI (B–Q). Scale bar, 100 μm.

(R–T) Reprogramming yield as defined by the number of $MAP2^+$, $TUJ1^+$, and $DAPI^+$ cells per frame of view (R, T), and reprogramming efficiency as defined by the ratio of $MAP2^+$/$DAPI^+$ cells or $TUJ1^+$/$DAPI^+$ cells (S) were quantified. n = 15 frames from 3 independent experiments for each condition. Data are represented as mean ± SD, *p < 0.05, ***p < 0.001. ns, non-significant, one-way ANOVA with Sidak test. The difference between AMp and AMnp is highlighted with a red line and red asterisks to indicate statistical significance. For Figure 1T, statistical significance was compared with the control group.

(U–V) Electrophysiological recordings showed that the neurons at day 40 had voltage-gated Na^+ and K^+ currents (U), as well as evoked action potentials in response to current injections (V).

by marked cell death (Figures S2D– S2I). The three lines of fetal lung fibroblasts had conversion yields and efficiencies at similarly high levels compared with that of AG22056 skin fibroblasts (Figures S2G–S2L), while one line of adult lung fibroblasts exhibited significantly less conversion and more cell death (Figures S2M and S2G–S2I). In addition to age, the sex of the cell donors had no consistent impact on the conversion. Decreased conversion was

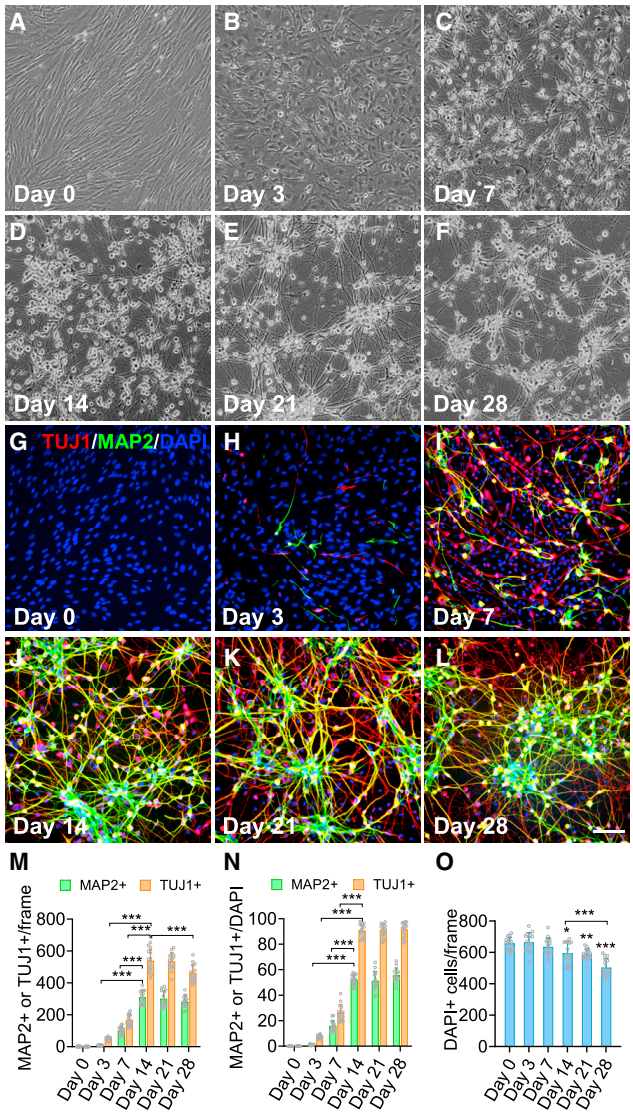

Figure 2. Reprogramming efficiency at different time points

(A–L) Phase contrast (A–F) and immunostaining (G–L) images of neurons induced with AMnp at different time points. Scale bar, 100 μm.

(M–O) Quantification of the number of MAP2$^+$, TUJ1$^+$. and DAPI$^+$ cells per frame of view (M, O), and the ratio of MAP2$^+$/DAPI$^+$ or TUJ1$^+$/DAPI$^+$ cells (N). n = 15 frames from 3 independent experiments for each condition. Data are represented as mean ± SD, *p < 0.05, **p < 0.01, ***p < 0.001. Statistical significance was determined by one-way ANOVA with Sidak test. For Figure 3O, statistical significance was compared with day 0.

strongly correlated to increased cell death, irrespective of age and sex of the donors.

Most of the AMnp-induced neurons are GABAergic

We stained AMnp-induced neurons at day 28 with antibodies against markers for various neuronal types and found that 71.1% ± 9.0% of MAP2$^+$ neurons were GABA$^+$ (Figures 3A and 3K). GABAergic neurons in the brain fall into three main groups that express parvalbumin (PV; approximately 40%), somatostatin (SST; approximately 30%), or serotonin receptor 3a (5HT3aR; approximately 30%) (Tremblay et al., 2016). We found that 79.1% ± 7.8% of the GABA$^+$ neurons were PV$^+$ (Figures 3B and 3K) and did not observe any SST$^+$ (Figure 3C) or 5HT3aR$^+$ cells (Figure 3D). In addition, 3.9% ± 1.4% of the MAP2$^+$ neurons were TH$^+$ (Figure 3E and 3K). We failed to detect the expression of the glutamatergic neuron markers VGlut1 and VGlut2 (Figures 3F and 3G), the serotonergic neuron marker 5-HT (Figure 3H), the cholinergic neuron marker ChAT (Figure 3I), or the striatal medium spiny neuron marker DARPP32 (D-32) (Figure 3J). The specificity of these antibodies was confirmed by positive and specific staining in rat brain sections (Figure S3). Quantitative RT-PCR (RT-qPCR) showed the marked induction of *GAD67* (Figure 3L) and *PV* (Figure 3M), the significant suppression of *SST* (Figure 3N), and the unchanged low expression of *5HT3aR* (Figure 3O) in AMnp-induced neurons at day 28 compared with control fibroblasts. Consistent with these results, longitudinal RNA-seq analyses (see below) showed the induction of many genes related to GABAergic neurons (Figure 3P) and the suppression of fibroblast genes (Figure 3Q).

Transcriptomic analysis identifies the induction of key RSRs

To gain mechanistic insights on how AMnp induced the efficient and rapid conversion of human skin fibroblasts to neurons, we performed RNA-seq analysis of cells at days 3, 7, and 14—three critical time points in the generation of increasingly more neurons (Figure 2). Indeed, we found increasing number of differentially expressed genes (DEGs) from day 3 to day 14, with 2,773 genes up-regulated and 1,648 genes down-regulated at day 14 (Figures 4A–4C; Table S2). Among them, 493 genes had continuously increased expression (AMnp_up) (Figure 4D; Table S3) and 104 genes had continuously decreased expression (AMnp_down) (Figure 4E and Table S3). The overlap of the 493 continuously up-regulated genes with the 305 RSRs that we have curated (Fisher and Feng, 2022) showed 7 RSRs with continuously increased expression (Figure 4F). Hierarchical clustering on the expression of all 305 RSRs across 52 human tissue types and 2 human cell lines from the GTEx database (Consortium, 2020) identified 11 brain-restricted RSRs (Figure S4). Five of the 7 continuously up-regulated RSRs (Figure 4F) were among the 11 brain-restricted RSRs (Figure 4H, marked by red asterisks). None of the 305 RSRs showed continuously decreased expression (Figure 4G). The 493 continuously up-regulated genes were enriched with Gene Ontology (GO) terms related to various neuronal processes, while the 104 continuously

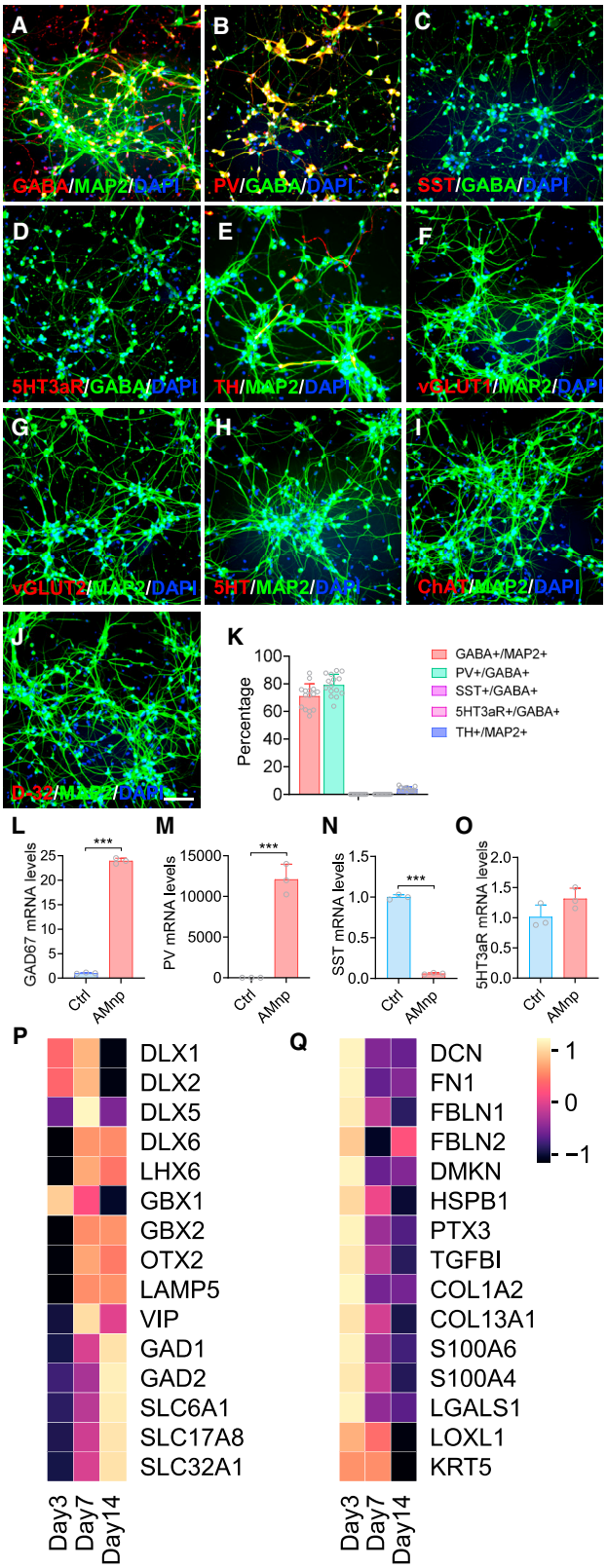

Figure 3. Most of the AMnp-induced neurons are GABAergic

(A–J) Co-staining of the induced neurons for MAP2 and GABAergic neuronal marker GABA (A); GABA and the GABAergic interneuron markers PV (B), SST (C), or 5-HT_3 serotonin receptor 5HT3aR (D); the dopaminergic neuron marker tyrosine hydroxylase (TH) (E); the glutamatergic neuron markers VGlut1 (F) or VGlut2 (G); the serotonergic neuron marker 5-HT (H); the cholinergic neuron marker choline acetyltransferase (ChAT) (I); or the medium spiny neuron marker DARPP32 (D-32) (J). Scale bar, 100 μm.

(K) The ratio of $GABA^+/MAP2^+$, $PV^+/GABA^+$, and $TH^+/MAP2^+$ cells at day 28. n = 15 frames from 3 independent experiments.

(L–O) RT-qPCR measurements of GAD67, PV, SST, and 5HT3aR mRNA levels from control fibroblasts and AMnp-induced neurons at day 28. n = 3 independent experiments. Data are represented as mean ± SD. ***p < 0.001. Statistical significance was determined by unpaired, two-tailed Student's t tests.

(P–Q) Heatmap showing normalized expression of genes related to GABAergic neurons (P) or fibroblasts (Q) at different time points of conversion.

down-regulated genes were associated with responses to virus (Figure 4I). It suggests that, as neuronal genes are induced, suppression of the antiviral response elicited by the lentiviral vectors may also be important for the trans-differentiation of skin fibroblasts to neurons. Given the importance of AS of RNA in neuronal development (Fisher and Feng, 2022; Weyn-Vanhentenryck et al., 2018), these results suggest that RSRs may play key roles in the conversion of skin fibroblasts to neurons.

To substantiate this idea, we performed RNA-seq on AG22056 cells being converted by Anp or AMp at days 3, 7, and 14 (Figure S5). In the absence of *MiR124*, Anp significantly and continuously induced five RSRs (*CELF5*, *CPEB3*, *ELAVL4*, *NOVA2*, and *RBFOX1*) (Figures S5A–S5F). In addition, AMp significantly and continuously induced 7 RSRs (*CELF4*, *CELF5*, *CPEB3*, *ELAVL4*, *NOVA2*, *RBFOX1*, and *RBFOX3*) (Figures S5H–S5M), despite the lack of *nPTB* shRNA. The induction of overlapping sets of RSRs by Anp, Amp, and AMnp shared very similar patterns (Figure S5O). Consistent with previous literature (Makeyev et al., 2007), the presence of *MiR124* indeed suppressed the expression of *PTBP1* significantly from day 3 to day 14 (Figure S5P), but only significantly reduced *PTBP2* expression at day 3 (Figure S5Q). Furthermore, the expression levels of *PTBP1* and *PTBP2* were quite constant from day 3 to day 14 (Figures S5P–S5Q). The results support the general induction of RSRs in the conversion of human skin fibroblasts to neurons, independent of the effect of *MiR124* on *PTBP1* or *PTBP2*.

RBFOX3 is critical for the AMnp-induced conversion of skin fibroblasts to neurons

As seven RSRs were continuously induced by AMnp, we overexpressed each one of them with AMp or AMnp. Six

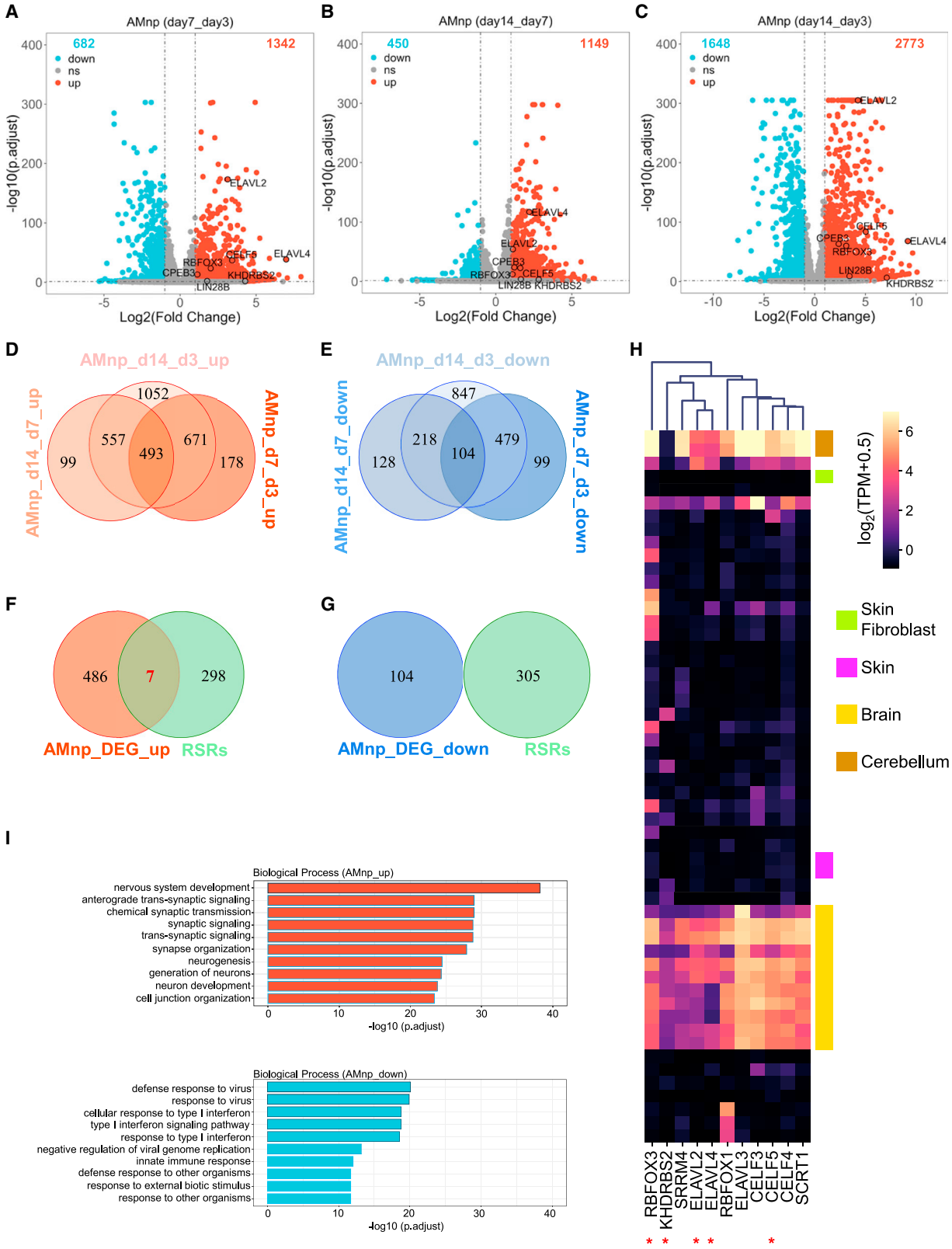

(legend on next page)

of the seven RSRs (*CELF5*, *CPEB3*, *ELAVL2*, *ELAVL4*, *LIN28B*, and *KHDRBS2*) decreased the conversion yields and efficiencies to various degrees in comparison with AMp or AMnp, respectively (Figure S6). Only the overexpression of *RBFOX3*, which encodes the mature neuronal marker NeuN (Dredge and Jensen, 2011; Kim et al., 2009), significantly increased the conversion yield of AMp from 113.1 ± 22.2 to 150.1 ± 32.9 $MAP2^+$ neurons per frame and from 257.3 ± 48.2 to 337.0 ± 69.8 $TUJ1^+$ cells per frame ($p < 0.001$) (Figures 5A, 5B, and 5G). The conversion efficiency was significantly increased from 18.6% ± 3.5% to 24.6% ± 5.6% for the $MAP2^+/DAPI^+$ ratio and from 42.2% ± 7.1% to 54.9% ± 10.2% for the $TUJ1^+/DAPI^+$ ratio ($p < 0.001$) (Figure 5H). *RBFOX3* (R3) did not significantly enhance the conversion efficiency of AMnp (R3+AMnp vs. AMnp: 51.4% ± 3.7% vs. 52.1% ± 4.0% for the $MAP2^+/DAPI^+$ ratio; 89.5% ± 4.2% vs. 90.5% ± 5.1% for the $TUJ1^+/DAPI^+$ ratio; $p > 0.05$) (Figures 5D, 5E, and 5H), suggesting that the enhancing effect of *RBFOX3* overexpression or *nPTB* knockdown on top of AMp occludes each other. Consistent with these data, *RBFOX3* knockdown significantly attenuated the transdifferentiation induced by AMp or AMnp (Figures S7A–S7F) and led to marked reduction of $DAPI^+$ cells, which was caused by cell death as evidenced by three independent staining for activated caspase 3, LIVE/DEAD, or Trypan Blue (Figures S7G–S7X).

The full-length *RBFOX3* containing exon 8 is highly expressed in neurons, while the truncated *RBFOX3* with exon 8 spliced out is expressed in non-neurons at a low level (Kim et al., 2013). Expression of the exon 8-deleted *RBFOX3* [R3(ΔE8)] significantly decreased the transdifferentiation induced by AMp (Figures 5C, 5G, and 5H) or AMnp (Figures 5F–5H). To substantiate the role of exon 8, we generated lentiviruses expressing shRNAs that targeted either the exon 8-included full-length *RBFOX3* (R3 E8in sh) or the exon 8-excluded truncated *RBFOX3* (R3 E8ex sh) (Figures 5J and 5K). Knocking down the endogenous full-length R3 significantly decreased the transdifferentiation induced by AMp (AMp+R3 E8in sh vs. AMp: 12.9% ± 2.6% vs. 18.6% ± 3.5% for the $MAP2^+/DAPI^+$ ratio; 28.3% ± 3.8% vs. 42.2% ± 7.1% for the $TUJ1^+/DAPI^+$ ratio; $p < 0.01$) (Figures 5M and 5S) or AMnp (AMnp+R3 E8in sh vs. AMnp: 42.0% ± 3.1% vs. 52.1% ± 4.0% for the $MAP2^+/DAPI^+$ ratio; 56.6% ± 4.9% vs. 90.6% ± 5.1% for the $TUJ1^+/DAPI^+$ ratio; $p < 0.001$) (Figures 5P and 5S). In contrast, knocking down the endogenous exon 8-excluded R3 did not significantly affect the conversions (Figures 5N, 5Q, and 5S). These results demonstrate the critical role of the full-length *RBFOX3*, which is generated by its neuron-specific AS, in the conversion.

nPTB knockdown promotes neuron-specific AS in concert with *RBFOX3*

The neuron-specific RSR *RBFOX3* (NeuN) promotes neuronal differentiation by regulating the AS of *Numb* (Kim et al., 2013) and *Ank3* (Jacko et al., 2018), which play pivotal roles in brain development. We examined whether *nPTB* knockdown affected the AS of exon 8 of *RBFOX3* using RT-PCR (Kim et al., 2013). As the skin fibroblasts were converted to neurons, the splicing pattern of *RBFOX3* shifted from the truncated isoform (excluding exon 8) to the full-length mRNA (including exon 8) (Figure 6A), which is necessary for neuronal differentiation (Kim et al., 2013). Quantification of percent spliced in (PSI) of this exon in AG22056 fibroblasts being converted by AMp or AMnp at different days showed an increased trend in the production of the full-length *RBFOX3* (Figure 6B). Both AMp and AMnp induce *RBFOX3* expression (Figure 6A). RT-qPCR showed that AMp induced significantly higher *RBFOX3* expression than AMnp did (Figure S5R). The results indicate that the induction of *RBFOX3* is independent of nPTB.

RT-PCR analysis and PSI quantification of splicing variants of a number of genes important for signal transduction and synaptic function also showed time-dependent, increased production of splicing isoforms favored in mature neurons. They included the $GABA_A$ receptor γ2 subunit *GABRG2* (Degener et al., 2022); the critical GABAergic synapse organizer *GPHN* (Choii and Ko, 2015); the receptor tyrosine kinase *ERBB4* (Wang et al., 2021), which is enriched in GABAergic interneurons (Fazzari et al., 2010; Vullhorst et al., 2009); the CaM kinase II β subunit *CAMK2B* (Li et al., 2014); the potassium channel

Figure 4. Transcriptomic analysis of induced neurons

(A–C) Volcano plots showing DEGs in cells converted by AMnp at different time points. DEGs are color coded by the legend. down, down-regulated; up, up-regulated; ns, non-significant. Continuously up-regulated RSRs are annotated.

(D and E) Venns diagram showing overlapping of up-regulated DEGs (D) and down-regulated DEGs (E) of AMnp at different time points. AMnp_d14_d7_up: up-regulated genes at day 14 vs. day 7; AMnp_d14_d7_down: down-regulated genes at day 14 vs. day 7.

(F and G) Venn diagrams showing overlapping of all RSRs with the 493 continuously up-regulated genes (F) or the 104 continuously down-regulated genes (G).

(H) Heatmap showing expression pattern of brain-restricted RSRs across tissues (see Figure S5 for full tissue annotation). *Genes among the 7 continuously up-regulated RSRs in (F).

(I) GO biological process analysis of the continuously up-regulated and down-regulated genes.

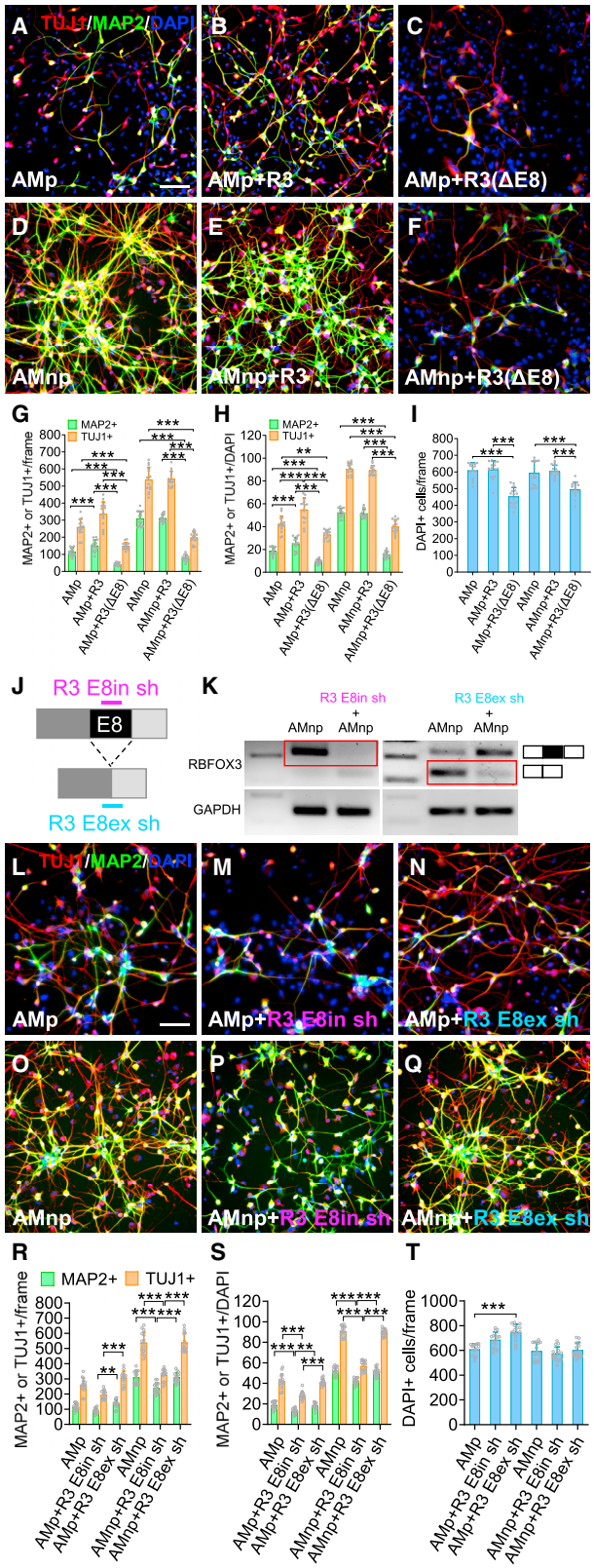

Figure 5. RBFOX3 is critical for the conversion

(A–F) AG22056 fibroblasts were reprogrammed with lentiviruses expressing AMp (A) and AMnp (D), plus the full-length RBFOX3 (R3) (B, E) or RBFOX3 with exon 8 deleted [R3(ΔE8)] (C, F) for 14 days and co-stained as indicated. Scale bar, 100 μm.

(G–I) Quantification of the number of MAP2$^+$, TUJ1$^+$ (G), or DAPI$^+$ (I) cells per frame, and the ratio of MAP2$^+$/DAPI$^+$ or TUJ1$^+$/DAPI$^+$ cells (H). n = 15 frames from 3 independent experiments for each condition, **p < 0.01, ***p < 0.001, one-way ANOVA with Sidak test.

(J) The location of the shRNA targeting the exon 8-included full-length *RBFOX3* (R3 E8in sh) or the shRNA targeting the exon 8-excluded *RBFOX3* (R3 E8ex sh).

(K) AG22056 fibroblasts were transduced with lentiviruses expressing AMnp plus R3 E8in sh or R3 E8ex sh for 3 days. RT-PCR showed splicing isoform-specific knockdown of *RBFOX3* by the two shRNAs.

(L–Q) AG22056 fibroblasts were reprogrammed with lentiviruses expressing AMp (L) and AMnp (O) plus R3 E8in sh (M, P), or R3 E8ex sh (N, Q) for 14 days and co-stained as indicated. Scale bar, 100 μm.

(R–T) Quantification of the number of MAP2$^+$, TUJ1$^+$ (R), or DAPI$^+$ (T) cells per frame, and the ratio of MAP2$^+$/DAPI$^+$ or TUJ1$^+$/DAPI$^+$ cells (S). n = 15 frames from 3 independent experiments for each condition, **p < 0.01, ***p < 0.001, one-way ANOVA with Sidak test.

KCNQ2 (Li et al., 2014); the membrane-cytoskeleton linker *ANK2* (Li et al., 2014); and the axon initial segment component *ANK3* (Li et al., 2014) (Figures 6A and 6B). At the same day of conversion, AMnp generally induced significantly higher expression of the neuronal isoforms of these genes compared with that induced by AMp (Figures 6A and 6B). These data suggest that *nPTB* knockdown enhances neuronal maturation by increasing the expression of neuron-specific AS isoforms of critical genes.

In addition to AMp or AMnp, *RBFOX3* knockdown significantly suppressed the production of neuron-specific AS isoforms of most the genes examined, while *RBFOX3* overexpression either significantly enhanced the production of some of these isoforms or did not elevate the favorable effects further (Figures 6C and 6D). These results are consistent with the effects of *RBFOX3* knockdown or overexpression in the AMp- or AMnp-induced transdifferentiation (Figure 5) and corroborate the critical role of *RBFOX3* in the conversion. *RBFOX3* overexpression or knockdown in combination with AMp did not appreciably affect the expression of endogenous *nPTB* (Figure 6C).

To understand the genome-wide splicing changes during the transdifferentiation, we identified AS events mediated by AMp and AMnp from RNA-seq data at days 3, 7, and 14. To compare them with the actual splicing patterns *in vivo*, we quantified AS events in human brains and skin fibroblasts from the GTEx database (Consortium, 2020) and identified the exon-exon junctions that were differentially spliced between human fibroblasts and brain and

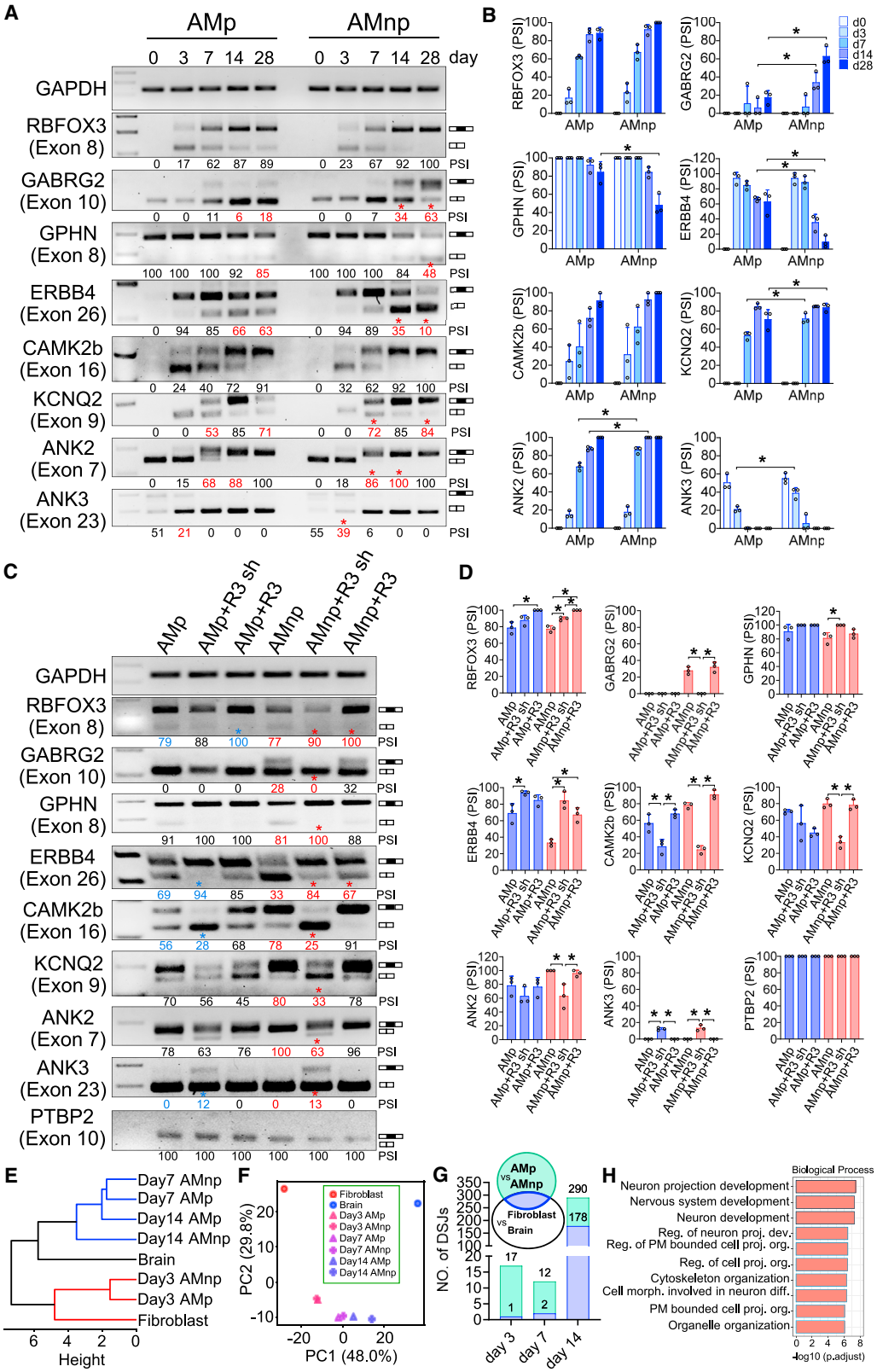

(legend on next page)

were also detected during transdifferentiation (Table S4). Both hierarchical clustering (Figure 6E) and principal component analysis (Figure 6F) showed that the RNA splicing profiles of cells induced by AMp or AMnp at day 3 resembled those of fibroblasts, while cells induced by AMnp at day 14 were closest to the brain. From day 7 to day 14, there was a dramatic increase in number of differentially spliced junctions (DSJs) that were common to the DSJs between AMp and AMnp, and the DSJs between fibroblast and brain (Figure 6G, blue bars). The genes that correspond with the 290 DSJs between AMp and AMnp on day 14 were functionally enriched in neural development (Figure 6H). These data indicate that *nPTB* knockdown pushed the global RNA splicing profile toward a brain-specific pattern, which facilitates the conversion to neurons.

DISCUSSION

The transdifferentiation of human skin fibroblasts to neurons is a valuable approach to study neurodegenerative disorders, such as Alzheimer's disease (Mertens et al., 2021) and Parkinson's disease (Xu et al., 2017), where patient-specific neurons can be generated quickly, while maintaining the epigenetic information imparted by age (Mertens et al., 2021). The usefulness of these applications stimulates effort to improve the conversion through a better understanding of the mechanism. The parallels between the transdifferentiation and the development of neuroepithelial cells to neurons can inform mechanistic investigations. The pioneer transcription factor ASCL1 plays a prominent role in both processes (Guillemot and Hassan, 2017). When ectopically expressed in a skin fibroblast, ASCL1 binds to the promoter of many critical genes involved in neurogenesis, even when these genes are in heterochromatin (Wapinski et al., 2013). It also induces the cyclin-dependent kinase inhibitor p27Kip1 (Farah et al., 2000) to cause cell-cycle exit within 1–2 days (Jiang et al., 2015). We observed no conversion in the absence of ASCL1 during the first 14 days (Figures 1D–1J and 1M). Indeed, it takes 4 weeks to convert human skin fibroblasts to a small percentage of $MAP2^{+}$ neurons with MIR9/9*-124 alone (Yoo et al., 2011), which is significantly enhanced by the addition of various transcription factors (Victor et al., 2014; Yoo et al., 2011). These results suggest that ASCL1 is a critical driver in transdifferentiation (Wapinski et al., 2013), while the actions of MIR9/9*-124 are significantly boosted by neurogenic transcription factors in the acquisition of specific neuronal fates (Abernathy et al., 2017; Victor et al., 2014; Yoo et al., 2011).

The brain-enriched MIR9/9*-124 exerts pleiotropic effects on the transdifferentiation process, including the suppression of REST, the switch of critical cofactors in the BAF chromatin remodeling complex, and the reduction of PTB and nPTB (Lu and Yoo, 2018). The downregulation of *nPTB* markedly increased the reprogramming efficiency and yield of A, AM, or AMp (Figure 1). The complex interactions between A, M, n, and p produced a synergy that improved not only the reprogramming efficiency and yield, but also the morphology and function of the induced neurons (Figure 1).

We found that the key reason for *nPTB* knockdown to significantly enhance the transdifferentiation induced by AMp seems to be the continuous induction of *RBFOX3* (Figure 4), an RSR that plays a critical role in the differentiation of neural progenitor cells to neurons (Zhang et al., 2016). *RBFOX3* knockdown markedly decreased the conversion induced by either AMp or AMnp (Figure S7), while overexpression of *RBFOX3* significantly enhanced AMp-induced transdifferentiation and occluded the beneficial effect of *nPTB* knockdown (Figure 5). The effect of *RBFOX3* relies on the neuron-specific full-length version containing

Figure 6. *PTBP2* knockdown enhances AS of genes that promote neuronal maturation

(A) The AS of the indicated genes were examined using RT-PCR in skin fibroblasts induced with AMp and AMnp for different days. Representative gel images are shown. The red numbers with asterisks indicate significant differences on the same day between AMp and AMnp, as quantified in (B).

(B) Quantification of PSI for neuron-enriched AS events from the RT-PCR gels. Shown are mean ± SD, n = 3, *p < 0.05. Statistical significance was determined by two-way ANOVA with Sidak test.

(C) RT-PCR analysis of the AS of the indicated genes in neurons induced by AMp or AMnp with or without *RBFOX3* shRNA (R3 sh) or overexpression of *RBFOX3* (R3) at day 14. Blue numbers with asterisks indicate significant differences in the AMp group, while red numbers and asterisks indicate significant differences in the AMnp group, as quantified in (D).

(D) Quantification of PSI for splicing events from the RT-PCR gels. Shown are mean ± SD, n = 3. *p < 0.05. Statistical significance was determined by one-way ANOVA with Sidak test.

(E–H) Bioinformatic analysis of genome-wide AS in the RNA-seq data of skin fibroblasts converted by AMp or AMnp for the indicated days. Hierarchical clustering (E) and principal component analysis (F) of fibroblast, brain and induced neurons at different days based on exon-exon junctions that were both detected in reprogramming and were differentially spliced between fibroblast and brain. Linkage in (E) was calculated by complete assigns with Euclidean distance. At the indicated days, the number of DSJs between cells induced by AMp or AMnp (teal colored) are overlapped with DSJs between fibroblast and brain (white color), with the overlap shown in blue color (G). The top 10 GO terms of the 290 DSJs at day 14 are shown in (H).

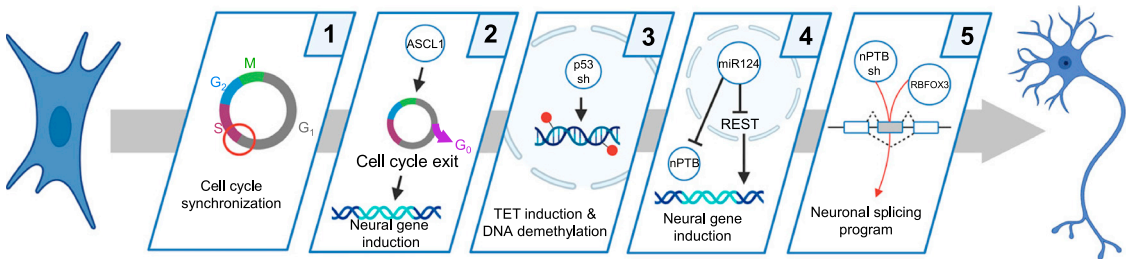

Figure 7. A sequential model for the transdifferentiation of human skin fibroblasts to neurons

(1) Synchronization of the cell cycle, by serum withdrawal, at the G1/S checkpoint makes the cells receptive to transdifferentiation.

(2) The pioneer transcription factor ASCL1 causes cell-cycle exit and induces neuronal genes.

(3) Knockdown of p53 induces the TET family of DNA demethylases to facilitate the epigenetic reprogramming.

(4) MIR-124 promotes the conversion through pleiotropic actions that include the suppression of REST and the reduced expression of nPTB via nonsense-mediated decay.

(5) nPTB knockdown and the induction of RBFOX3 during the conversion work in concert to drive a neuronal AS program that improves the transdifferentiation.

exon 8, since overexpression of exon 8-excluded truncated *RBFOX3* markedly decreased conversions induced by AMp or AMnp (Figure 5). Consistent with this, splicing isoform-specific knockdown of full-length *RBFOX3* significantly decreased the conversion, while knocking down exon 8-excluded truncated *RBFOX3* did not significantly affect the transdifferentiation (Figure 5). In developing mouse and human brains, RBFOX3 orchestrates the AS of many neurogenesis genes to change microtubule organization, cortical actin, and postsynaptic proteins (Zhang et al., 2016). Interestingly, 61% of the alternatively spliced exons have common motifs that can be recognized by Ptbp1/2 and Rbfox1/2/3 families of RSRs, where the two families act antagonistically to regulate the AS of key neuronal genes (Zhang et al., 2016). Indeed, neuron-specific AS of many genes was suppressed by *RBFOX3* knockdown and enhanced by *RBFOX3* overexpression (Figures 6C and 6D). Thus, we propose that *nPTB* knockdown and *RBFOX3* act in concert.

Most of the AMnp-induced neurons were GABAergic (Figure 3). Several factors contribute to this. ASCL1 plays an important role in the development of GABAergic neurons (Fode et al., 2000; Parras et al., 2002) in the ventral forebrain (Lim et al., 2018). In addition, the regulation of AS is a key determinant of neuronal identity (Fisher and Feng, 2022). Distinct splicing programs between GABAergic and glutamatergic neurons are controlled by overlapping sets of exons (Feng et al., 2021). PTBP2 is a crucial RSR in the expression of $GABA_A$ receptors during development (Li et al., 2014). MiR124 upregulates both *Ptbp2* and *Gabbr1* ($GABA_B$ receptor 1) expression (Makeyev et al., 2007). Indeed, AMp-induced conversion was accompanied by a coordinated AS program of the GABAergic gene battery, including the $GABA_A$ receptor γ2 subunit *GABRG2* (Degener et al., 2022), the critical GABAergic synapse organizer *GPHN* (Choii and Ko, 2015), and the receptor tyrosine kinase *ERBB4* (Wang et al., 2021), which is enriched in GABAergic interneurons (Fazzari et al., 2010; Vullhorst et al., 2009) (Figures 6A and 6B). Knockdown of *nPTB* enhanced this coordinated AS program to facilitate the conversion and maturation of GABAergic neurons. *RBFOX3* knockdown greatly attenuated this AS program, while *RBFOX3* overexpression did not further enhance the effect of *nPTB* knockdown (Figures 6C and 6D). Interestingly, tissue-specific deletion of *Rbfox3* in mice shows the greatest defects when *Rbfox3* is knocked out in GABAergic neurons. The loss of *Rbfox3* in GABAergic neurons decreases the number of these neurons and causes abnormal GABAergic transmission and seizures (Huang et al., 2022). The rapid generation of patient-specific induced GABAergic neurons enables applications, such as biomarker discovery and drug screening, for many brain disorders that involve GABAergic neurons.

In conclusion, our study supports a sequential model to understand how human skin fibroblasts are transdifferentiated to neurons in a rapid and efficient manner (Figure 7). First, cell-cycle synchronization at the G1/S checkpoint induced by serum withdrawal arrests the attention of mitotic cells to extracellular and intracellular stimuli, instead of running a mitotic program focused on when to copy genomic DNA (Jiang et al., 2015). Second, overexpression of ASCL1 forces a rapid exit from the cell cycle (Farah et al., 2000; Jiang et al., 2015), while inducing the expression of many neuronal genes (Wapinski et al., 2013). Third, these epigenetic changes are aided by *p53* knockdown, which induces the TET family of DNA demethylases (Jiang et al., 2015). Fourth, the induction of neuronal genes is facilitated by *MIR9/9*-124*, which suppresses the expression of *REST* and *nPTB* (Lu and Yoo, 2018). Suppression of *REST* enhances the expression of neuronal genes that are

normally repressed in skin fibroblasts. Fifth, the attenuation of nPTB by *nPTB* shRNA and overexpression of *MIR9/9*-124* changes the AS program from that of a fibroblast to a neuron. Among the numerous genes that are continuously up-regulated, *RBFOX3* plays a critical and specific role in the conversion by promoting the neuron-specific AS program. The other continuously up-regulated RSRs play diverse roles in neurogenesis, but not in this particular conversion (Figure S6). For example, the deletion of ELAVL2 in the mouse retina produces a specific reduction of amacrine cells (Wu et al., 2021a). Similarly, ELAVL4 knockout mice show a transient impairment in the development of several cranial nerves at the embryonic stage (Akamatsu et al., 2005). The actions of RSRs seem to be context specific.

EXPERIMENTAL PROCEDURES

Resource availability

Corresponding author

Jian Feng: jianfeng@buffalo.edu.

Materials availability

All data are reported in the paper or deposited in GEO. Materials can be released via a material transfer agreement.

Data and code availability

All RNA-seq data in this study are deposited in GEO: GSE210131. Our code is available at GitHub: https://github.com/fenglabbuf/2023_Zhu_et_al.

Materials

pLKO.1/*p53*shRNA (#19119), pLKO.1/scrambled shRNA (#1864), pMD2.G (#12259), psPAX2 (#12260), and pTight-9-124-BclxL (miR9/9*-124, #60857) were from Addgene. FUW-tetO-LoxP-ASCL1 and FUW-LoxP-M2rtTA were generated previously (Jiang et al., 2015). Human *PTBP2*, *BRN2*, *MYT1L*, *NEUROND1*, *RBFOX3*, *ELAVL2*, *ELAVL4*, *CELF5*, *CPEB3*, *LIN28B*, and *KHDRBS2* ORFs were from Addgene or Genscript, then subcloned to the FUW-tetO-LoxP lentiviral vector. pLKO.1/shRNA (*PTBP2*, TRCN0000001111; *RBFOX3*, TRCN0000254935) were selected from TRC (RNAi Consortium) shRNA library (Moffat et al., 2006) and shRNA for *RBFOX3* E8in (GCTGAATGGGACGATCGTAGA) and *RBFOX3* E8ex (GGGGCTCCAAGGTCAATAATGC) were cloned into pLKO.1.

FUW-RBFOX3 (ΔE8) construction

To construct FUW-RBFOX3 (ΔE8), the *RBFOX3* gene fragment exons 1–7 and exons 9–15 were PCR amplified using primer pair RBFOX3-F1/RBFOX3-R1 or RBFOX3-F2/RBFOX3-R2 from vector FUW-RBFOX3, respectively. The exons 1–7 and exons 9–15 fusion fragments were obtained by overlap PCR using primer pair RBFOX3-F1/RBFOX3-R2 and cloned into the FUW vector. The construct was confirmed by sequencing. Primers used for overlapping PCR are listed in Table S1.

Cell culture

Primary human fibroblast lines include skin fibroblasts: AG22056 (newborn foreskin, male, Coriell Institute), AG04451 (16 gestational weeks, female, Coriell Institute), GM00726 (26 years of age, female, Coriell Institute), AG16146 (31 years of age, male, Coriell Institute), GM09918 (78 years of age, male, Coriell Institute), and GM00731 (96 years of age, male, Coriell Institute); lung fibroblasts: MRC5 (14 gestational weeks, male, American Type Culture Collection [ATCC]), AG04452 (16 gestational weeks, female, Coriell Institute), IMR90 (16 gestational weeks, female, ATCC), and AG02603 (35 years of age, female, Coriell Institute). All fibroblasts were maintained in DMEM (Gibco, 11965092) with 10% FBS (Gibco, 10437028), 100 U/mL penicillin, 100 μg/mL streptomycin, 0.1 mM NEAA, and 2 mM L-glutamine at 37°C. All cell cultures were regularly tested for the absence of mycoplasma by PCR (Zhang et al., 2021).

Transdifferentiation of human fibroblasts to neurons

Fibroblasts were seeded on a Matrigel (Corning, 354277)-coated 12-well plate (5×10^4 cells per well) and incubated at 37°C in 5% CO_2 for 16 h. The next day, cells were infected with the indicated lentiviruses at multiplicity of infection (MOI) of 10 for each virus in the presence of 8 μg/mL polybrene (Sigma, H9268). After 16 h, virus-containing medium was removed and cells were washed three times with DMEM/F12 medium (Gibco, 11330032) to remove serum and cultured in DMEM/F12 without serum for 24 h to arrest the cell cycle at the G1/S checkpoint, when the cells are most receptive to reprogramming (Jiang et al., 2015). The following day (day 0), medium was changed to neural induction medium (DMEM/F12, 1 × N2, 1 × B27, 0.1 mM non-essential amino acid, 0.5 μM dorsomorphin [Tocris, 3093], 2.5 μM SB431542 [Tocris, 1614], 1 μM PD0332991 [Tocris, 4786], 3 μM CHIR99021 [Tocris, 4423], 0.2 mM vitamin C [Sigma, A4544], 10 μM Y27632 [Tocris, 1254], 0.5 mM db-cAMP [ApexBio, B9001], 20 ng/mL nerve growth factor [PeproTech, 450-01], 20 ng/mL glial cell line-derived neurotrohic factor [PeproTech, 450-10], 20 ng/mL brain-dervied neurotrophic factor [PeproTech, 450-02], and 1 μg/mL doxycycline [Tocris, 4090]). Cells were maintained at 37°C in 5% CO_2 and 5% O_2. The medium was changed every other day for the duration of the culture period.

More than 99.9% of the human fibroblasts were infected when one lentivirus was applied at an MOI of 10 (Jiang et al., 2015). Thus, when we used AMnp together with M2rtTA, the probability of a cell infected by all five lentiviruses was more than 99.5% (0.999^5). This was corroborated by the lack of any cell death in puromycin. The pLKO.1 lentiviral vector for the knockdown of *nPTB* and *p53* contains a puromycin resistance gene.

Immunostaining

Immunocytochemistry was performed as described previously (Jiang et al., 2015) with antibodies listed in Table S1. Fluorescence images were generated on a Leica AF6000 Inverted Microscope. Cells were counted from 15 randomly selected fields at 10× magnification for each condition from three independent experiments. LIVE/DEAD cell viability assay (Invitrogen, catalog #R37601) was performed according to the manufacturer's instruction.

RT-qPCR

RT-qPCR measurements of gene expression in total RNA was performed as described previously (Jiang et al., 2015) with the primers

listed in Table S1. PCR products separated in 2% gels were quantified using Quantity one software (Bio-Rad). PSI was calculated as follows: Intensity of inclusion band/(Intensity of inclusion band + Intensity of exclusion band).

Electrophysiology

AG22056 cells were seeded on poly-L-ornithine (Sigma, P4638)/Matrigel-coated plastic coverslips (Thermo Fisher Scientific, 174969), transduced with lentiviruses expressing AMnp, and cultured for 40 days. To record action potentials (APs), whole-cell patch-clamp were performed with the internal solution containing: 125 mM K-gluconate, 10 mM KCl, 10 mM HEPES, 0.5 mM EGTA, 3 mM Na_2ATP, 0.5 mM Na_2GTP, and 12 mM phosphocreatine, pH 7.25, 280 mOsm on a Multiclamp 700A amplifier and Digidata1322A data acquisition system (Molecular Devices). In current-clamp mode, cells were perfused with artificial cerebrospinal fluid (ACSF), and the resting membrane potentials were held at −65 mV. APs were elicited by step injection currents ranging from 0 to 90 pA at 10-pA intervals. To record voltage-dependent sodium and potassium currents, the same internal solution was used. Cells held at −70 mV were perfused with ACSF. Currents were recorded at the step membrane potential ranging from −70 to 30 mV at 10-mV intervals. Data were analyzed in Clampfit (Molecular Devices).

RNA-seq and bioinformatic analysis

RNA-seq was performed from three biological replicates at days 3, 7, and 14. Libraries were constructed using TruSeq stranded RNA library prep (Illumina) and NovaSeq 6000 SP reagent kit (Illumina). Sequencing was performed on the NovaSeq 6000 platform (Illumina) with 50-bp paired-end reads at the Genomics and Bioinformatics Core of the State University of New York at Buffalo. RNA-seq data were trimmed by Cutadapt (Kechin et al., 2017) (version 1.16) to remove low-quality 4-bp regions at the start and discard reads with mapping quality less than 20, then aligned to hg38 reference genome (University of California Santa Cruz) by HISAT2 (Afgan et al., 2018; Kim et al., 2019) (galaxy version 2.1.0). Counts of fragments aligned to genes annotated on the reference genome (RefSeq Release 109.20201120) were generated by featureCounts (Liao et al., 2014) (subreads version 2.0.1). Normalized counts for genes and statistical tests of DEGs were analyzed using DESeq2 (Love et al., 2014) package (version 1.32.0) in R. DEGs were defined as adjusted $p < 0.05$ and $|\log_2(\text{fold change})|>1$ between two groups being compared. Volcano plots were generated using ggplot2 package (version 3.3.5). GO analysis was performed using ClusterProfiler package (Wu et al., 2021b) (version 4.5.2).

To analyze tissue-specific RSR expression, processed RNA-seq data of 52 human tissue types and 2 human cell lines (skin fibroblasts and Epstein-Barr virus-transformed lymphocytes) as medium TPM across 17382 samples were downloaded from the genotype tissue expression (GTEx) Consortium (v8 release, https://gtexportal.org/home/datasets) (Consortium, 2020). The medium TPM values of all 305 RSRs (Fisher and Feng, 2022) included in the dataset were log2 transformed with a pseudocount of 0.5, then hierarchical clustering and visualization were performed with Python library Seaborn (https://seaborn.pydata.org/).

To quantify splicing event, STAR (Dobin et al., 2013) (version 2.7.10a) was used to align the reads to hg38 reference genome and generate junction read counts. Junction read counts of RNA-seq on human skin fibroblast (n = 504) and brain (n = 2642) samples were downloaded from the GTEx Consortium (Dobin et al., 2013). All junction read counts were formatted to be processed by LeafCutter (Li et al., 2018) for calculating PSI and providing statistical significance reports of intron clusters between two groups of samples. DSJs were defined as Benjamini-Hochberg corrected p value of <0.05 and $|\Delta PSI|>0.1$ between two groups being compared. Hierarchical clustering was performed with Python package SciPy. Principal component analysis was performed with Python package scikit-learn.

Statistical analysis

Data were analyzed with GraphPad Prism 8 and expressed as the mean ± SD. One- or two-way ANOVA and the Student's t test were used for statistical analyses. Statistical report and raw data for all figures are in Table S5.

SUPPLEMENTAL INFORMATION

Supplemental information can be found online at https://doi.org/10.1016/j.stemcr.2023.09.012.

ACKNOWLEDGMENTS

The work is supported in part by the U.S. Department of Veterans Affairs Merit Award BX002452 (J.F.) and the National Institutes of Health grant NS113763 (J.F.).

AUTHOR CONTRIBUTIONS

B.Z. and J.F. conceived the project; B.Z. and E.F. performed all conversion experiments and analyzed the data; L.L. performed bioinformatics analysis of the RNA-seq data; P.Z. performed the electrophysiology experiments under the guidance of Z.Y. All authors contributed to the writing and editing of the manuscript.

DECLARATION OF INTERESTS

The authors declare no competing interests.

Received: October 27, 2022
Revised: September 19, 2023
Accepted: September 20, 2023
Published: October 12, 2023

REFERENCES

Abernathy, D.G., Kim, W.K., McCoy, M.J., Lake, A.M., Ouwenga, R., Lee, S.W., Xing, X., Li, D., Lee, H.J., Heuckeroth, R.O., et al. (2017). MicroRNAs Induce a Permissive Chromatin Environment that Enables Neuronal Subtype-Specific Reprogramming of Adult Human Fibroblasts. Cell Stem Cell *21*, 332–348.e9.

Afgan, E., Baker, D., Batut, B., van den Beek, M., Bouvier, D., Cech, M., Chilton, J., Clements, D., Coraor, N., Grüning, B.A., et al. (2018). The Galaxy platform for accessible, reproducible and collaborative biomedical analyses: 2018 update. Nucleic Acids Res. *46*, W537–W544.

Akamatsu, W., Fujihara, H., Mitsuhashi, T., Yano, M., Shibata, S., Hayakawa, Y., Okano, H.J., Sakakibara, S.I., Takano, H., Takano, T., et al. (2005). The RNA-binding protein HuD regulates neuronal cell identity and maturation. Proc. Natl. Acad. Sci. USA. *102*, 4625–4630.

Choii, G., and Ko, J. (2015). Gephyrin: a central GABAergic synapse organizer. Exp. Mol. Med. *47*, e158.

Aguet, F., Anand, S., Ardlie, K.G., Gabriel, S., Getz, G.A., Graubert, A., Hadley, K., Handsaker, R.E., Huang, K.H., Kashin, S., et al. (2020). The GTEx Consortium atlas of genetic regulatory effects across human tissues. Science *369*, 1318–1330.

DeFelipe, J., Alonso-Nanclares, L., and Arellano, J.I. (2002). Microstructure of the neocortex: comparative aspects. J. Neurocytol. *31*, 299–316.

Degener, M.J.F., van Cruchten, R.T.P., Otero, B.A., Wang, E.T., Wansink, D.G., and 't Hoen, P.A.C. (2022). A comprehensive atlas of fetal splicing patterns in the brain of adult myotonic dystrophy type 1 patients. NAR Genom. Bioinform. *4*, lqac016.

Dobin, A., Davis, C.A., Schlesinger, F., Drenkow, J., Zaleski, C., Jha, S., Batut, P., Chaisson, M., and Gingeras, T.R. (2013). STAR: ultrafast universal RNA-seq aligner. Bioinformatics *29*, 15–21.

Dredge, B.K., and Jensen, K.B. (2011). NeuN/Rbfox3 nuclear and cytoplasmic isoforms differentially regulate alternative splicing and nonsense-mediated decay of Rbfox2. PLoS One *6*, e21585.

Farah, M.H., Olson, J.M., Sucic, H.B., Hume, R.I., Tapscott, S.J., and Turner, D.L. (2000). Generation of neurons by transient expression of neural bHLH proteins in mammalian cells. Development *127*, 693–702.

Fazzari, P., Paternain, A.V., Valiente, M., Pla, R., Luján, R., Lloyd, K., Lerma, J., Marín, O., and Rico, B. (2010). Control of cortical GABA circuitry development by Nrg1 and ErbB4 signalling. Nature *464*, 1376–1380.

Feng, H., Moakley, D.F., Chen, S., McKenzie, M.G., Menon, V., and Zhang, C. (2021). Complexity and graded regulation of neuronal cell-type-specific alternative splicing revealed by single-cell RNA sequencing. Proc. Natl. Acad. Sci. USA. *118*, e2013056118.

Feng, J. (2016). Kinetic barriers in transdifferentiation. Cell Cycle *15*, 1019–1020.

Fisher, E., and Feng, J. (2022). RNA splicing regulators play critical roles in neurogenesis. Wiley Interdiscip. Rev. RNA *13*, e1728.

Fode, C., Ma, Q., Casarosa, S., Ang, S.L., Anderson, D.J., and Guillemot, F. (2000). A role for neural determination genes in specifying the dorsoventral identity of telencephalic neurons. Genes Dev. *14*, 67–80.

Guillemot, F., and Hassan, B.A. (2017). Beyond proneural: emerging functions and regulations of proneural proteins. Curr. Opin. Neurobiol. *42*, 93–101.

Huang, D.F., Lee, C.Y., Chou, M.Y., Yang, T.Y., Cao, X., Hsiao, Y.H., Wu, R.N., Lien, C.C., Huang, Y.S., Huang, H.P., et al. (2022). Neuronal splicing regulator RBFOX3 mediates seizures via regulating Vamp1 expression preferentially in NPY-expressing GABAergic neurons. Proc. Natl. Acad. Sci. USA. *119*, e2203632119.

Jacko, M., Weyn-Vanhentenryck, S.M., Smerdon, J.W., Yan, R., Feng, H., Williams, D.J., Pai, J., Xu, K., Wichterle, H., and Zhang, C. (2018). Rbfox Splicing Factors Promote Neuronal Maturation and Axon Initial Segment Assembly. Neuron *97*, 853–868.e6.

Jiang, H., Xu, Z., Zhong, P., Ren, Y., Liang, G., Schilling, H.A., Hu, Z., Zhang, Y., Wang, X., Chen, S., et al. (2015). Cell cycle and p53 gate the direct conversion of human fibroblasts to dopaminergic neurons. Nat. Commun. *6*, 10100.

Kechin, A., Boyarskikh, U., Kel, A., and Filipenko, M. (2017). cutPrimers: A New Tool for Accurate Cutting of Primers from Reads of Targeted Next Generation Sequencing. J. Comput. Biol. *24*, 1138–1143.

Kim, D., Paggi, J.M., Park, C., Bennett, C., and Salzberg, S.L. (2019). Graph-based genome alignment and genotyping with HISAT2 and HISAT-genotype. Nat. Biotechnol. *37*, 907–915.

Kim, K.K., Adelstein, R.S., and Kawamoto, S. (2009). Identification of neuronal nuclei (NeuN) as Fox-3, a new member of the Fox-1 gene family of splicing factors. J. Biol. Chem. *284*, 31052–31061.

Kim, K.K., Nam, J., Mukouyama, Y.S., and Kawamoto, S. (2013). Rbfox3-regulated alternative splicing of Numb promotes neuronal differentiation during development. J. Cell Biol. *200*, 443–458.

Li, H., Jiang, H., Yin, X., Bard, J.E., Zhang, B., and Feng, J. (2019). Attenuation of PRRX2 and HEY2 enables efficient conversion of adult human skin fibroblasts to neurons. Biochem. Biophys. Res. Commun. *516*, 765–769.

Li, Q., Zheng, S., Han, A., Lin, C.H., Stoilov, P., Fu, X.D., and Black, D.L. (2014). The splicing regulator PTBP2 controls a program of embryonic splicing required for neuronal maturation. Elife *3*, e01201.

Li, Y.I., Knowles, D.A., Humphrey, J., Barbeira, A.N., Dickinson, S.P., Im, H.K., and Pritchard, J.K. (2018). Annotation-free quantification of RNA splicing using LeafCutter. Nat. Genet. *50*, 151–158.

Liao, Y., Smyth, G.K., and Shi, W. (2014). featureCounts: an efficient general purpose program for assigning sequence reads to genomic features. Bioinformatics *30*, 923–930.

Lim, L., Mi, D., Llorca, A., and Marín, O. (2018). Development and Functional Diversification of Cortical Interneurons. Neuron *100*, 294–313.

Lipscombe, D., and Lopez Soto, E.J. (2019). Alternative splicing of neuronal genes: new mechanisms and new therapies. Curr. Opin. Neurobiol. *57*, 26–31.

Love, M.I., Huber, W., and Anders, S. (2014). Moderated estimation of fold change and dispersion for RNA-seq data with DESeq2. Genome Biol. *15*, 550.

Lu, Y.L., Liu, Y., McCoy, M.J., and Yoo, A.S. (2021). MiR-124 synergism with ELAVL3 enhances target gene expression to promote neuronal maturity. Proc. Natl. Acad. Sci. USA. *118*, e2015454118.

Lu, Y.L., and Yoo, A.S. (2018). Mechanistic Insights Into MicroRNA-Induced Neuronal Reprogramming of Human Adult Fibroblasts. Front. Neurosci. *12*, 522.

Makeyev, E.V., Zhang, J., Carrasco, M.A., and Maniatis, T. (2007). The MicroRNA miR-124 promotes neuronal differentiation by triggering brain-specific alternative pre-mRNA splicing. Mol. Cell *27*, 435–448.

Melé, M., Ferreira, P.G., Reverter, F., DeLuca, D.S., Monlong, J., Sammeth, M., Young, T.R., Goldmann, J.M., Pervouchine, D.D.,

Sullivan, T.J., et al. (2015). Human genomics. The human transcriptome across tissues and individuals. Science *348*, 660–665.

Mertens, J., Herdy, J.R., Traxler, L., Schafer, S.T., Schlachetzki, J.C.M., Böhnke, L., Reid, D.A., Lee, H., Zangwill, D., Fernandes, D.P., et al. (2021). Age-dependent instability of mature neuronal fate in induced neurons from Alzheimer's patients. Cell Stem Cell *28*, 1533–1548.e6.

Moffat, J., Grueneberg, D.A., Yang, X., Kim, S.Y., Kloepfer, A.M., Hinkle, G., Piqani, B., Eisenhaure, T.M., Luo, B., Grenier, J.K., et al. (2006). A lentiviral RNAi library for human and mouse genes applied to an arrayed viral high-content screen. Cell *124*, 1283–1298.

Pang, Z.P., Yang, N., Vierbuchen, T., Ostermeier, A., Fuentes, D.R., Yang, T.Q., Citri, A., Sebastiano, V., Marro, S., Südhof, T.C., and Wernig, M. (2011). Induction of human neuronal cells by defined transcription factors. Nature *476*, 220–223.

Parras, C.M., Schuurmans, C., Scardigli, R., Kim, J., Anderson, D.J., and Guillemot, F. (2002). Divergent functions of the proneural genes Mash1 and Ngn2 in the specification of neuronal subtype identity. Genes Dev. *16*, 324–338.

Tremblay, R., Lee, S., and Rudy, B. (2016). GABAergic Interneurons in the Neocortex: From Cellular Properties to Circuits. Neuron *91*, 260–292.

Victor, M.B., Richner, M., Hermanstyne, T.O., Ransdell, J.L., Sobieski, C., Deng, P.Y., Klyachko, V.A., Nerbonne, J.M., and Yoo, A.S. (2014). Generation of human striatal neurons by microRNA-dependent direct conversion of fibroblasts. Neuron *84*, 311–323.

Vierbuchen, T., and Wernig, M. (2011). Direct lineage conversions: unnatural but useful? Nat. Biotechnol. *29*, 892–907.

Vullhorst, D., Neddens, J., Karavanova, I., Tricoire, L., Petralia, R.S., McBain, C.J., and Buonanno, A. (2009). Selective expression of ErbB4 in interneurons, but not pyramidal cells, of the rodent hippocampus. J. Neurosci. *29*, 12255–12264.

Wang, Z., Chan, H.W., Gambarotta, G., Smith, N.J., Purdue, B.W., Pennisi, D.J., Porrello, E.R., O'Brien, S.L., Reichelt, M.E., Thomas, W.G., and Paravicini, T.M. (2021). Stimulation of the four isoforms of receptor tyrosine kinase ErbB4, but not ErbB1, confers cardiomyocyte hypertrophy. J. Cell. Physiol. *236*, 8160–8170.

Wapinski, O.L., Vierbuchen, T., Qu, K., Lee, Q.Y., Chanda, S., Fuentes, D.R., Giresi, P.G., Ng, Y.H., Marro, S., Neff, N.F., et al. (2013). Hierarchical mechanisms for direct reprogramming of fibroblasts to neurons. Cell *155*, 621–635.

Weyn-Vanhentenryck, S.M., Feng, H., Ustianenko, D., Duffié, R., Yan, Q., Jacko, M., Martinez, J.C., Goodwin, M., Zhang, X., Hengst, U., et al. (2018). Precise temporal regulation of alternative splicing during neural development. Nat. Commun. *9*, 2189.

Wu, M., Deng, Q., Lei, X., Du, Y., and Shen, Y. (2021a). Elavl2 Regulates Retinal Function Via Modulating the Differentiation of Amacrine Cells Subtype. Invest. Ophthalmol. Vis. Sci. *62*, 1.

Wu, T., Hu, E., Xu, S., Chen, M., Guo, P., Dai, Z., Feng, T., Zhou, L., Tang, W., Zhan, L., et al. (2021b). clusterProfiler 4.0: A universal enrichment tool for interpreting omics data. Innovation *2*, 100141.

Xu, Z., Chu, X., Jiang, H., Schilling, H., Chen, S., and Feng, J. (2017). Induced dopaminergic neurons: A new promise for Parkinson's disease. Redox Biol. *11*, 606–612.

Xu, Z., Su, S., Zhou, S., Yang, W., Deng, X., Sun, Y., Li, L., and Li, Y. (2020). How to reprogram human fibroblasts to neurons. Cell Biosci. *10*, 116.

Xue, Y., Ouyang, K., Huang, J., Zhou, Y., Ouyang, H., Li, H., Wang, G., Wu, Q., Wei, C., Bi, Y., et al. (2013). Direct conversion of fibroblasts to neurons by reprogramming PTB-regulated microRNA circuits. Cell *152*, 82–96.

Xue, Y., Qian, H., Hu, J., Zhou, B., Zhou, Y., Hu, X., Karakhanyan, A., Pang, Z., and Fu, X.D. (2016). Sequential regulatory loops as key gatekeepers for neuronal reprogramming in human cells. Nat. Neurosci. *19*, 807–815.

Yoo, A.S., Sun, A.X., Li, L., Shcheglovitov, A., Portmann, T., Li, Y., Lee-Messer, C., Dolmetsch, R.E., Tsien, R.W., and Crabtree, G.R. (2011). MicroRNA-mediated conversion of human fibroblasts to neurons. Nature *476*, 228–231.

Zhang, B., Li, H., Hu, Z., Jiang, H., Stablewski, A.B., Marzullo, B.J., Yergeau, D.A., and Feng, J. (2021). Generation of mouse-human chimeric embryos. Nat. Protoc. *16*, 3954–3980.

Zhang, X., Chen, M.H., Wu, X., Kodani, A., Fan, J., Doan, R., Ozawa, M., Ma, J., Yoshida, N., Reiter, J.F., et al. (2016). Cell-Type-Specific Alternative Splicing Governs Cell Fate in the Developing Cerebral Cortex. Cell *166*, 1147–1162.e15.